A DEFORMABLE MODEL FOR THE RECONSTRUCTION OF THE NEONATAL CORTEX

Andreas Schuh[1], Antonios Makropoulos[1], Robert Wright[2], Emma C. Robinson[1], Nora Tusor[3], Johannes Steinweg[3], Emer Hughes[3], Lucilio Cordero Grande[2], Anthony Price[3], Jana Hutter[2], Joseph V. Hajnal[2], Daniel Rueckert[1]

[1]Department of Computing, Imperial College London, London, UK
[2]Department of Biomedical Engineering, Kings College London, London, UK
[3]Department of Perinatal Imaging & Health, King's College London, London, UK

ABSTRACT

We present a method based on deformable meshes for the reconstruction of the cortical surfaces of the developing human brain at the neonatal period. It employs a brain segmentation for the reconstruction of an initial inner cortical surface mesh. Errors in the segmentation resulting from poor tissue contrast in neonatal MRI and partial volume effects are subsequently accounted for by a local edge-based refinement. We show that the obtained surface models define the cortical boundaries more accurately than the segmentation. The surface meshes are further guaranteed to not intersect and subdivide the brain volume into disjoint regions. The proposed method generates topologically correct surfaces which facilitate both a flattening and spherical mapping of the cortex.

Index Terms— deformable, neonatal, cortex, surface

1. INTRODUCTION

A prerequisite for the analysis of brain scans is to obtain models of the cortex [1]. Such models can be extracted from T1-weighted (T1w) adult brain images using free software, e.g., FreeSurfer [2], Caret [3], and BrainSuite [4]. Due to different signal properties of the immature brain and the need for a shortened scan time, MR sequences developed for the adult brain cannot be used. A T2-weighted (T2w) sequence further gives better tissue contrast for structural analysis. Aforementioned tools can thus not directly be used and instead rely on a custom segmentation of the neonatal brain image. Automatic segmentations often contain errors, however, because of poor tissue contrast owing to the shortened acquisition, partial volume, and need for motion correction. Partial volume averaging often causes cerebrospinal fluid (CSF) being mislabelled as either white matter (WM) or cortical grey matter (cGM).

Our method can reconstruct the inner (WM) and outer (pial) cortical surfaces of the neonatal brain. Unlike our previous method [5], we only utilise a segmentation to obtain an initial surface mesh that is refined using a novel edge-based force which corrects aforementioned segmentation errors.

2. BRAIN SEGMENTATION

Our method builds upon a previous bias field correction, a segmentation of the brain into WM, GM, and CSF, along with a segmentation of deep grey matter (dGM) structures, the lateral ventricles, brainstem (BS) and cerebellum (CB). For this we employ the Draw-EM [6] package[1] of the MIRTK[2].

Given the Draw-EM labels of right and left structures, we determine two orthogonal cutting planes. The first cutting plane separates the structures of the right and left cerebral hemispheres and is found by principle component analysis of the covariance matrix of inter-hemispheric border voxels. The second plane is defined to be orthogonal to this medial cutting plane. With the plane normal fixed, we find a plane distance from the origin such that it cuts through the superior part of the brainstem, separating brainstem and cerebellum from the cerebrum. Morphological closing of the dGM structures is done to include voxels labelled as CSF and intra-cranial background within the sub-cortical neighbourhood. We then partition the volume into right and left cerebrum, cortex, and brainstem plus cerebellum.

3. SURFACE RECONSTRUCTION

3.1. White matter surface

For each brain hemisphere, we compute the convex hull of the boundary of its corresponding cerebrum mask. This convex hull is a closed genus-0 surface, i.e., of desired spherical topology. This initial triangular mesh is deformed inwards towards the zero level set of the implicit surface given by the signed Euclidean distance transform of the segmentation.

The employed deformable WM surface model is governed by a simplified version of the Lagrange equations of motion in discrete form, which are integrated with a simple forward Euler scheme,

$$\mathbf{x}_i(t + dt) = \mathbf{x}_i(t) + \mathbf{f}_i(t)dt \quad (1)$$

[1]https://biomedia.doc.ic.ac.uk/software/draw-em/
[2]https://biomedia.doc.ic.ac.uk/software/mirtk/

where $\mathbf{x}_i(t)$ is the position of node i at time point t, dt is the Euler integration step length, and $\mathbf{f}_i(t) = w_d\mathbf{f}_i^s(t)+w_b\mathbf{f}_i^b(t)+w_g\mathbf{f}_i^g(t)+w_r\mathbf{f}_i^r(t)$ is the weighted sum of the external and internal forces acting on node i as defined in the following, with positive weights $w_{\{d,b,g,r\}}$. At each iteration, the force $\mathbf{f}_i$ is, for each node individually, either halved a pre-set maximum number of times or set to zero if the resulting surface mesh would self-intersect after the Euler step. This is to enforce a hard non-self-intersection constraint.

To allow the discrete surface to locally contract or expand, local adaptive remeshing operations such as edge-melting and triangle subdivision are performed after each Euler step [7].

3.1.1. *External force*

The external force, $\mathbf{f}^s$, attracts the surface towards the segmentation boundary and is given by

$$\mathbf{f}_i^s = m_i^s \times \mathbf{n}_i \tag{2}$$

where $\mathbf{n}_i$ is the surface normal at node i, and $m_i^s = \operatorname{sgn} d_i^s \times \operatorname{smf}(|d_i^s|, 0, d_{max})$ the signed magnitude given the distance, d_i^s, of the node to the segmentation boundary in normal direction. The S-shaped membership function smf is used to normalise the force magnitude from $[a, b]$ to $[0, 1]$, i.e.,

$$\operatorname{smf}(x,a,b) = \begin{cases} 0, & \text{if } x \le a \\ 2\left(\frac{x-a}{b-a}\right)^2, & \text{if } a < x \le \frac{a+b}{2} \\ 1-2\left(\frac{x-b}{b-a}\right)^2, & \text{if } \frac{a+b}{2} < x < b \\ 1, & \text{if } x \ge b \end{cases} \tag{3}$$

The distance d_i^s is computed by finding the closest intersection with the segmentation along a ray cast in both inwards and outwards normal direction. To reduce the influence of small irregularities in the segmentation boundary, a Laplacian smoothing of surface distances is performed with weights $w_{ij} = \max(0, \langle \mathbf{n}_i, \mathbf{n}_j \rangle)$ if nodes i and j are adjacent and $w_{ij} = 0$ otherwise. Small holes in the segmentation manifest themselves in this surface distance map as small clusters of supposedly distant points as seen left of Fig. 1. These are filled in to avoid the surface mesh to deform into them. Specifically, surface clusters are formed by growing regions starting at a seed node k that has not been assigned to a cluster yet s.t. $\forall i, |d_k^s| \ge |d_i^s|$. The region growing stops when either the surface distance drops below a predefined threshold or the angle made up by the normal vectors of the seed node and the propagating front node exceeds a specified threshold. This process is repeated until no more seed nodes have an absolute surface distance $|d_i^s| > d_{thres}$. Clusters which are elongated or have an excessively large radius are then removed. The segmentation boundary distance of nodes belonging to the remaining clusters is set to zero, followed by a few Laplacian smoothing iterations whereby only modified distance values are being updated. The effect of this is shown right in Fig. 1.

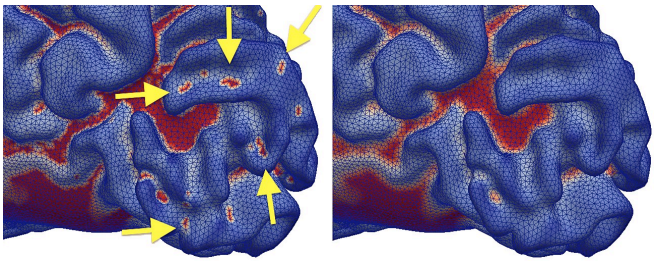

Fig. 1: WM segmentation boundary distance in normal direction, before clustering based hole filling (left), and after the hole filling and smoothing (right). A number of holes in the segmentation are indicated by yellow arrows.

3.1.2. *Internal forces*

Smoothness of the deformed surface is encouraged by the bending force, $\mathbf{f}^b$, which minimises curvature by attracting a node towards the barycentre of its adjacent nodes [7], i.e.,

$$\mathbf{f}_i^b(t) = \bar{\mathbf{x}}_i - \mathbf{x}_i - \frac{1}{N_i}\sum_{j=1}^{N_i}(\bar{\mathbf{x}}_{ij} - \mathbf{x}_{ij}) \tag{4}$$

where N_i is the number of nodes adjacent to node i and $\bar{\mathbf{x}}_i = \frac{1}{N_i}\sum_{j=1}^{N_i}\mathbf{x}_{ij}$ is the centroid of adjacent nodes ij.

An additional Gauss curvature based spring force, $\mathbf{f}^g$, avoids the creation of unwanted creases perpendicular to the length of a sulcus. Similar to $\mathbf{f}^b$, it attracts nodes to the barycentre of adjacent nodes, but with magnitude proportional to the Gauss curvature. Nodes with negative Gauss curvature, such as near the crest of unwanted creases between two gyri, are attracted only by adjacent nodes below or above the tangent plane, i.e.,

$$\mathbf{f}_i^g = m_i^g \times \bar{\mathbf{f}}_i^g \;/\; \left\|\bar{\mathbf{f}}_i^g\right\| \tag{5}$$

$$\bar{\mathbf{f}}_i^g = \frac{\sum_{j=1}^{N_i}\delta_{ij}^g \times (\mathbf{x}_{ij} - \mathbf{x}_i)}{\sum_{j=1}^{N_i}\delta_{ij}^g} \tag{6}$$

where δ_{ij}^g is an indicator function which, for negative Gauss curvature K_i, is 1 only for points on one side of the tangent plane at node i. Which side depends on the sign of the external force $\mathbf{f}_i^s$ that is positive for nodes inside the implicit target surface and negative outside of it. Hence, crest points with a negative Gauss curvature outside the segmentation are forced inwards, while points with a negative Gauss curvature inside the segmentation are forced outwards, i.e., $\delta_{ij}^g = \max(0, \operatorname{sgn} m_i^s \times \operatorname{sgn}\langle \mathbf{x}_{ij} - \mathbf{x}_i, \mathbf{n}_i \rangle)$ if $K_i < 0$ and $\delta_{ij}^g = 1$ otherwise. The magnitude of the spring force is $m_i^g = \operatorname{smf}(|K_i|, K_{min}, K_{max})$, where K_{min} and K_{max} are positive thresholds. The force is zero for $|K_i| < K_{min}$.

The internal force, $\mathbf{f}^r$, reduces the occurrence of self-intersections that have to be resolved after each Euler step by having nodes repel each other. It is proportional to the pairwise distance of the nodes and the dot product of their surface

normal vectors, such that nodes belonging to close opposing triangles repel each other stronger than nodes of triangles of the same surface patch with similar surface normals, i.e.,

$$\begin{aligned} \mathbf{f}_i^r &= \sum_{j=1}^{N} m_{ij}^r \times \frac{\mathbf{x}_i - \mathbf{x}_j}{\|\mathbf{x}_i - \mathbf{x}_j\|} \qquad (7) \\ m_{ij}^r &= \begin{cases} s_{ij}^r \left(\frac{\|\mathbf{x}_i - \mathbf{x}_j\|}{r} - 1 \right)^2, & \text{if } \|\mathbf{x}_i - \mathbf{x}_j\| < r \\ 0, & \text{otherwise} \end{cases} \\ s_{ij}^r &= \mathrm{smf}(-\langle \mathbf{n}_i, \mathbf{n}_j \rangle, 0, 1) \end{aligned}$$

The factor s_{ij}^r is zero for normal vectors that make up an angle of less or equal $90°$. Note that the terms of the sum in Eq. 7 are non-zero only for nodes j within a radius r of node i.

3.1.3. Combined surface mesh

We merge the right and left WM surface meshes at the medial cut to form one closed genus-0 surface. This surface mesh is further merged with the surface of the joined BS and CB segment at the previously introduced brainstem cut. In doing so, we ensure that individual surfaces do not intersect each other during and after the inflation of this combined, non-self-intersecting surface towards the pial surface. Triangles of the combined mesh are assigned labels identifying them as part of right cerebrum, left cerebrum, or brainstem and cerebellum.

3.2. Edge-based refinement

Draw-EM occasionally assigns CSF voxels within sulci incorrect WM or GM labels due to partial volume effects or averaging which takes place during motion correction. These wrongly labelled voxels cause the previous surface to not deform completely into narrow sulci. We therefore use a second model to refine the surface based on image intensities alone. The external force $\mathbf{f}_i^s$ is therefore replaced by $\mathbf{f}_i^e$ which attracts node i towards the closest WM/cGM edge in normal direction in the bias corrected image. For this, the segmentation boundary distance, d_i^s, in Eq. 2 is substituted by the WM/cGM edge distance, d_i^e. This distance is found by analysing the one-dimensional (1D) intensity profile and directional derivative sampled at equally spaced normal ray points. Two examples are shown in Fig. 2. A WM surface edge occurs between a maximum with WM intensity, followed by a minimum with cGM intensity (left/right of green vertical line). Starting at the ray center (red vertical line; yellow dot), we search for a suitable edge both inwards and outwards from the node until either a WM/cGM edge is found, a maximum search depth is exceeded, or the ray intersects the surface. The outwards search is stopped when an opposing cGM/WM or cGM/CSF edge is encountered. If a suitable edge was found only inwards or outwards, it is selected. Otherwise, the combined probability of both maximum and minimum intensities to belong to the WM and cGM class, respectively, are

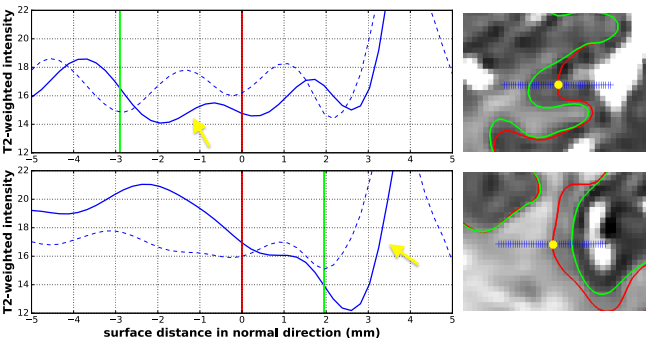

Fig. 2: Intensity (left; blue) and derivative (left; dashed) sampled from the image (right) at points marked by blue crosses. A yellow dot on the right marks the node on the initial surface (red). The green contour depicts the final WM surface. The arrows on the left show the cGM/CSF edge of the pial surface.

used to choose one of the two candidate edges. To encourage the surface to deform into deep sulci and skip CSF voxels encountered inside the current surface, the inwards edge is preferred whenever a cGM/CSF edge is found inside. These edges are identified by a minimum in the intensity profile followed by a maximum with an intensity above the WM mean intensity plus five times the standard deviation of WM intensities. The image edge distance d_i^e is equal the signed distance to the strongest minimum of the directional intensity derivative. A median filtering followed by Laplacian smoothing of edge distances mitigates errors caused by incorrectly identified edges due to noise and other image artefacts. The external force of adjacent nodes is further averaged, whereby the number of averaging steps is halved after convergence followed by a new Euler integration as previously proposed for the flattening and inflation in FreeSurfer [8]. This allows entire regions to move coherently in the appropriate direction.

3.3. Pial surface

The pial surface is obtained from the WM surface by deforming it towards the cGM/CSF interface. To ensure that the pial surface is strictly outside the WM surface, we first duplicate the cortical mesh nodes and deform these outwards in normal direction a few steps up to a maximum distance from the WM surface. This is done so the non-self-intersection constraint does not prevent the nodes from moving outwards from the original surface mesh. We then use an external force similar to $\mathbf{f}^e$ which, starting from the already reconstructed WM surface, searches for the closest cGM/CSF image edge instead. These edges correspond to a positive derivative in normal direction of the T2w intensity (arrows in Fig. 2). When no such edge is found, e.g., within a narrow sulcus due to partial volume effects, both opposing gyral folds expand towards each other until stopped by the non-self-intersection constraint.

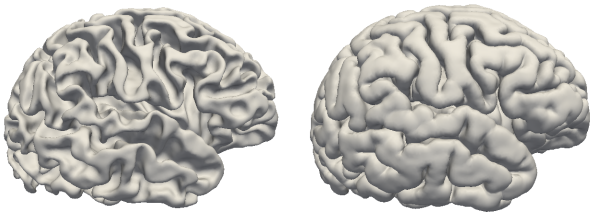

Fig. 3: Lateral views of white (left) and pial (right) surfaces.

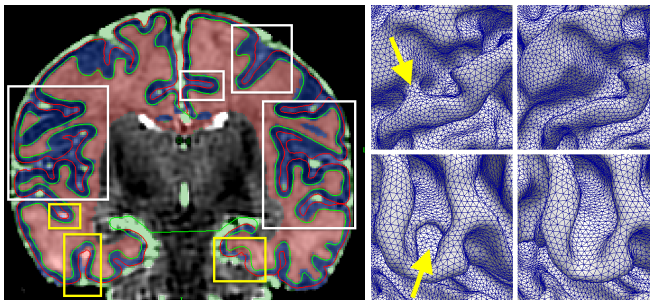

Fig. 4: Segmented T2w image intersected by white and pial surfaces (left). Zoom of white surface mesh before (middle) and after (right) edge-based refinement. See text for details.

4. RESULTS

We applied the proposed method to reconstruct the cortex of 71 neonates. The post menstrual age at scan ranges from 34.4 to 43.4 weeks with mean 39.6 weeks. We visually inspected the reconstructed surfaces. Exemplary renders of the reconstructed surfaces of one subject are shown in Fig. 3. An intersection of these with a coronal slice of the T2w image is shown left in Fig. 4. This image is overlayed with the WM (red), cGM (blue), and CSF (green) segmentation. It can be observed that the WM surface follows the WM/cGM interface also where CSF has been mislabelled as WM (yellow boxes). The pial surface further depicts the cGM/CSF boundary more truthfully then the cGM segmentation where CSF appears dark due to partial volume effects (white boxes). The effect of the edge-based refinement of the WM surface is shown on the right of Fig. 4. The top row shows an incorrect gyrus within the superior temporal sulcus resulting from misclassified CSF which was successfully "flattened". The bottom row shows a case where a large hole in the segmentation of the central sulcus resulted in a narrow WM surface, stopped only from self-intersecting by the non-self-intersection constraint, and is filled after the refinement.

5. CONCLUSION

We presented a method for reconstructing the neonatal cortex using deformable models of spherical topology. Errors in the segmentation are corrected for by an edge-based refinement based on hard-coded rules to find nearby edges. In future work, we will quantify our results and generate training data with the proposed approach, with manual correction where needed, and use machine learning to replace hard-coded rules. Our method is publicly available in MIRTK[3].

6. ACKNOWLEDGEMENTS

This work has received funding from the European Research Council under the European Unions Seventh Framework Programme (FP/2007-2013)/ERC Grant Agreement no. 319456. We are grateful to the families who generously supported this trial. The work was supported by the NIHR Biomedical Research Centers at Guys and St Thomas NHS Trust.

7. REFERENCES

[1] MF Glasser, SN Sotiropoulos, JA Wilson, TS Coalson, B Fischl, JL Andersson, J Xu, S Jbabdi, M Webster, JR Polimeni, DC Van Essen, and M Jenkinson, "The minimal preprocessing pipelines for the Human Connectome Project," *NeuroImage*, vol. 80, pp. 105–124, 2013.

[2] AM Dale, B Fischl, and MI Sereno, "Cortical surface-based analysis I: Segmentation and surface reconstruction," *NeuroImage*, vol. 9, no. 2, pp. 179–194, 1999.

[3] DC Van Essen, "Cortical cartography and Caret software," *NeuroImage*, vol. 62, no. 2, pp. 757–764, 2012.

[4] DW Shattuck and RM Leahy, "BrainSuite: An automated cortical surface identification tool," *Med. Image Anal.*, vol. 6, no. 2, pp. 129–142, 2002.

[5] R Wright, A Makropoulos, V Kyriakopoulou, PA Patkee, LM Koch, MA Rutherford, JV Hajnal, D Rueckert, and P Aljabar, "Construction of a fetal spatio-temporal cortical surface atlas from in utero MRI: Application of spectral surface matching," *NeuroImage*, vol. 120, pp. 467–480, 2015.

[6] A Makropoulos, IS Gousias, C Ledig, P Aljabar, A Serag, JV Hajnal, AD Edwards, SJ Counsell, and D Rueckert, "Automatic whole brain MRI segmentation of the developing neonatal brain," *IEEE Trans. Med. Imaging*, vol. 33, no. 9, pp. 1818–31, 2014.

[7] JY Park, T Mcinerney, D Terzopoulos, and MH Kim, "A non-self-intersecting adaptive deformable surface for complex boundary extraction from volumetric images," *Comput. Graph.*, vol. 25, pp. 421–440, 2001.

[8] B Fischl, MI Sereno, and AM Dale, "Cortical surface-based analysis II: Inflation, flattening, and a surface-based coordinate system," *NeuroImage*, vol. 9, no. 2, pp. 195–207, 1999.

[3] https://github.com/MIRTK/Deformable